

Crystal Engineering of 1D Exciton Systems Composed of Single- and Double-Stranded Perylene Bisimide J-Aggregates

Matthias Stolte, Reinhard Hecht, Zengqi Xie, Linlin Liu, Christina Kaufmann, Astrid Kudzus, David Schmidt, and Frank Würthner*

Single crystals of three at bay area tetraphenoxy-substituted perylene bisimide dyes are grown by vacuum sublimation. X-ray analysis reveals the self-assembly of these highly twisted perylene bisimides (PBIs) in the solid state via imide–imide hydrogen bonding into hydrogen-bonded PBI chains. The crystallographic insights disclose that the conformation and sterical congestion imparted by the phenoxy substituents can be controlled by *ortho*-substituents. Accordingly, whilst sterically less demanding methyl and isopropyl substituents afford double-stranded PBI chains of complementary *P* and *M* atropo-enantiomers, single hydrogen-bonded chains of homochiral PBIs are observed for the sterically more demanding *ortho*-phenyl substituents. Investigation of the absorption and fluorescence properties of microcrystals and thin films of these PBIs allow for an unambiguous interpretation of these exciton systems. Thus, the J-aggregates of the double-stranded crystals exhibit a much larger (negative) exciton coupling than the single-stranded one, which in contrast has the higher solid-state fluorescence quantum yield.

control of coloristic properties to afford high grade color pigments with hues from red to maroon by tuning the lateral and rotational displacement of the cofacially stacked chromophores.^[10] Based on the knowledge acquired by this research, more recently PBI packing arrangements could be tailored to provide outstanding n-channel organic semiconductor materials for organic transistors and solar cells.^[11–13] However, with their outstanding optical properties including fluorescence quantum yields up to unity,^[14] PBIs are interesting candidates for a broad variety of photonic applications as well.^[15–17] In this regard it is important that most recent research recognized for a variety of covalent and supramolecular PBI dimers as well as larger self-assembled PBI dye aggregates that, depending on the mutual arrange-

1. Introduction

Crystal engineering of π -scaffolds in general^[1–6] and of perylene bisimides (PBIs) in particular^[7–9] has a long tradition. For several decades PBI functional material research was focused on the

ment of the PBIs, entirely different photophysical properties can be tailored.^[18–20] These insights from small model systems now motivate the engineering of unprecedented PBI packing arrangements in solid-state materials with the goal to tailor functional properties for applications of these dyes beyond their conventional ones as color pigments.^[21–25] Here of particular interest is the longitudinal slip-stack arrangement of the dyes that affords dye aggregates with significant bathochromic shifts of the absorption and emission bands and high exciton mobilities originating from J-type exciton coupling.^[26] Accordingly, the aim of this work was to engineer a slip-stacked packing arrangement of PBI dyes to afford a new class of PBI pigments with solid-state properties that are distinguished from the common cofacially stacked color pigment materials.

Dr. M. Stolte, Dr. R. Hecht, Dr. C. Kaufmann, A. Kudzus, Dr. D. Schmidt, Prof. F. Würthner


Institut für Organische Chemie
Universität Würzburg
Am Hubland, Würzburg 97074, Germany
E-mail: wuerthner@uni-wuerzburg.de

Dr. M. Stolte, Dr. R. Hecht, Dr. C. Kaufmann, A. Kudzus, Dr. D. Schmidt, Prof. F. Würthner

Center for Nanosystems Chemistry (CNC) and Bavarian Polymer Institute (BPI)

Universität Würzburg
Theodor-Boveri-Weg, Würzburg 97074, Germany

Prof. Z. Xie, Prof. L. Liu
Institute of Polymer Optoelectronic Materials and Devices and State Key Laboratory of Luminescent Materials and Devices
South China University of Technology
Guangzhou 510640, P. R. China

 The ORCID identification number(s) for the author(s) of this article can be found under <https://doi.org/10.1002/adom.202000926>.

© 2020 The Authors. Published by WILEY-VCH Verlag GmbH & Co. KGaA, Weinheim. This is an open access article under the terms of the Creative Commons Attribution License, which permits use, distribution and reproduction in any medium, provided the original work is properly cited.

In our previous work, we applied the concept of hydrogen bond directed self-assembly to the class of at bay area four-fold phenoxy-substituted PBIs (**Figure 1**). By this, well-defined J-aggregates could be achieved with stacking motifs from double- up to sextuple-stranded helices in solution,^[27,28] in gels,^[29,30] and in the liquid-crystalline state.^[31–33] In-depth photophysical studies for these J-aggregates revealed highly desired properties including outstanding fluorescence quantum yields up to 90%, strong exciton coupling, and exciton migration for distances up to 100 nm.^[34,35] However, because all of these dye aggregates had to be equipped with long aliphatic or oligoethylene glycol chains for solubilization purpose, they are rather model systems than useful materials for desirable applications.

DOI: 10.1002/adom.202000926

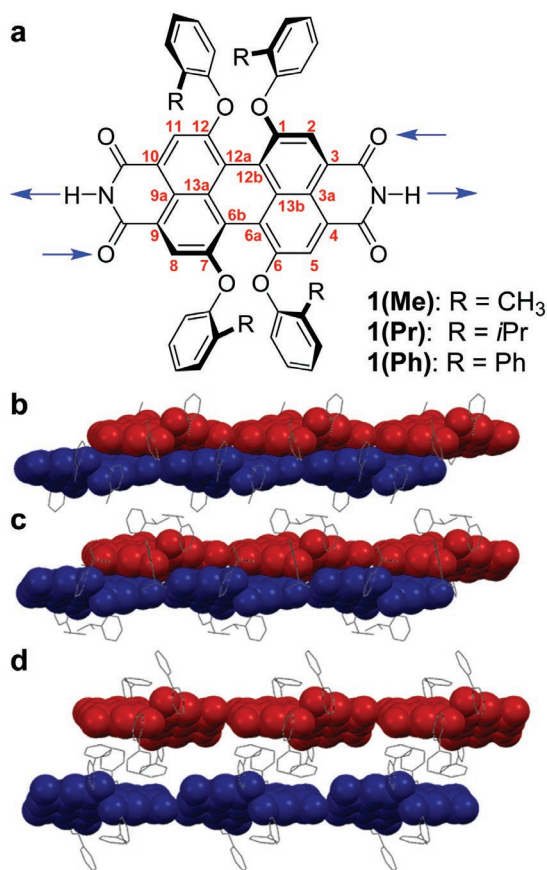


Figure 1. a) Chemical structure (*P* atropo-enantiomer) of the three investigated tetraphenoxy-substituted PBI dyes **1(Me)**, **1(Pr)**, and **1(Ph)** with labeling of the carbon atoms of the chromophore core (red) and hydrogen bonding pattern (blue arrows). Side view onto (b,c) the double- and (d) single-stranded packing arrangements of hydrogen-bonded PBIs b) **1(Me)**, c) **1(Pr)**, and d) **1(Ph)** in their respective single crystal structures. The PBI chromophores of *P* and *M* atropo-enantiomers are highlighted in blue and red, respectively.

Furthermore, it is noteworthy that the assignment of the number of self-assembled strands in these aggregates remained only tentative because neither for the aggregates in solution nor for those in the liquid-crystalline state an unambiguous structure determination by single crystal X-ray diffraction was possible. In addition, we were wondering how the helical packing structures considered for these self-assembled materials, i.e., each hydrogen-bonded aggregate fiber consisted of exclusively either *P* or *M* PBI atropo-enantiomers to give *P* and *M* helices (which are present in equal amounts in the columnar LC phases) could lead to crystalline unit cells.

2. Results and Discussion

For our current study we synthesized three at bay area tetraphenoxy-substituted PBIs **1(Me)**,^[29] **1(Pr)**, and **1(Ph)** (Figure 1) from methylbenzyl-protected 1,6,7,12-tetrachloro PBI with three distinct phenol derivatives and subsequent deprotection of the imide positions with boron tribromide (for details on synthesis and characterization see Supporting Information). By

using either a methyl, *iso*-propyl or phenyl substituent in *ortho*-position of the phenoxy group, the sterical demand around the π -scaffold of the chromophores is varied. It is noteworthy that the tetraphenoxy-substituted PBIs exhibit high conformational flexibility which improves the solubility of the otherwise insoluble pigment.^[36] However, this feature renders the crystallization of these dyes challenging. Accordingly, different from earlier (unsuccessful) attempts^[29,32] here crystallization was carried out on silicon wafer pieces in vacuum by thermal gradient sublimation at 305–330 °C and a pressure of $<2 \times 10^{-6}$ mbar, thereby exploiting the rapid interconversion of the various conformational states at elevated temperatures (Figure S1, Supporting Information). As another advantage of this method, the otherwise common inclusion of solvent molecules in the crystal lattice could be avoided and high-quality solvent-free single crystals suitable for single crystal X-ray analysis as well as spectroscopic investigations could be obtained (Figure 2).

The molecular structures of **1(Me)**, **1(Pr)**, and **1(Ph)** in the single crystals are depicted in Figure 2. What becomes immediately apparent from these molecular structures is a broken symmetry, i.e., in all cases the dihedral angles of two bay areas are unequal (for more details, see Supporting Information) and also the orientation of the *ortho*-substituents is not the same for the four phenoxy substituents. Due to the sterical congestion of the four phenoxy substituents, the twist angle between the two naphthalene units rises from about 24.5° for **1(Me)**, over 26.2° for **1(Pr)** up to 29.5° for **1(Ph)** with increasing size of the *ortho*-substituents (Table 1). This trend of increasing the inherent twist of the chromophore's π -scaffold is also measurable by the increasing dihedral angles for the four bay $\angle(\text{C1-C12b-C12a-C12})$ and four inner carbon atoms $\angle(\text{C13a-C12a-C12b-C13b})$ up to 32.8° and 26.9° for **1(Ph)**, respectively (for numbering see Figure 1a).

The increasing sterical demand of these substituents has another interesting effect on the molecular arrangement in the solid state: While the broken symmetry of **1(Me)** and **1(Pr)** affords one shielded π -surface and another one accessible for π - π interactions with neighboring molecules, such intermolecular π - π interactions are completely prohibited in case of **1(Ph)**. Here, the phenyl-residues fully surround the PBI core with one of them even attaching to the PBI surface by π - π interactions (3.62 Å; Figure 2c).

However, nothing influences the solid-state packing as strongly as the propensity of the PBI dyes to interact with each other by imide-imide hydrogen bonding, ranging from 2.83 to 2.94 Å between the oxygen and nitrogen atoms of the C=O...H-N units (Table 1). Thus, all imide units connect by twofold hydrogen bonding to neighbor molecules, leading to the line-up of the PBI molecules in 1D hydrogen-bonded supramolecular polymer chains (Figure 3). These strands always consist exclusively either of *P* (blue colored molecules) or *M* (red colored molecules) enantiomers, respectively, with neighboring strands always containing the opposite stereoisomer. In the case of **1(Me)** and **1(Pr)** the two neighboring single-strands are attached closely at van der Waals distances of about 3.48–3.51 Å (Table 1) between slip-stacked, longitudinally displaced PBI molecules, thereby affording a textbook example for J-aggregates with slip angle ($\theta_{\text{center-center}}$) of about 25.4°–29.8° (Figure 3 and Table 1). It is important to emphasize

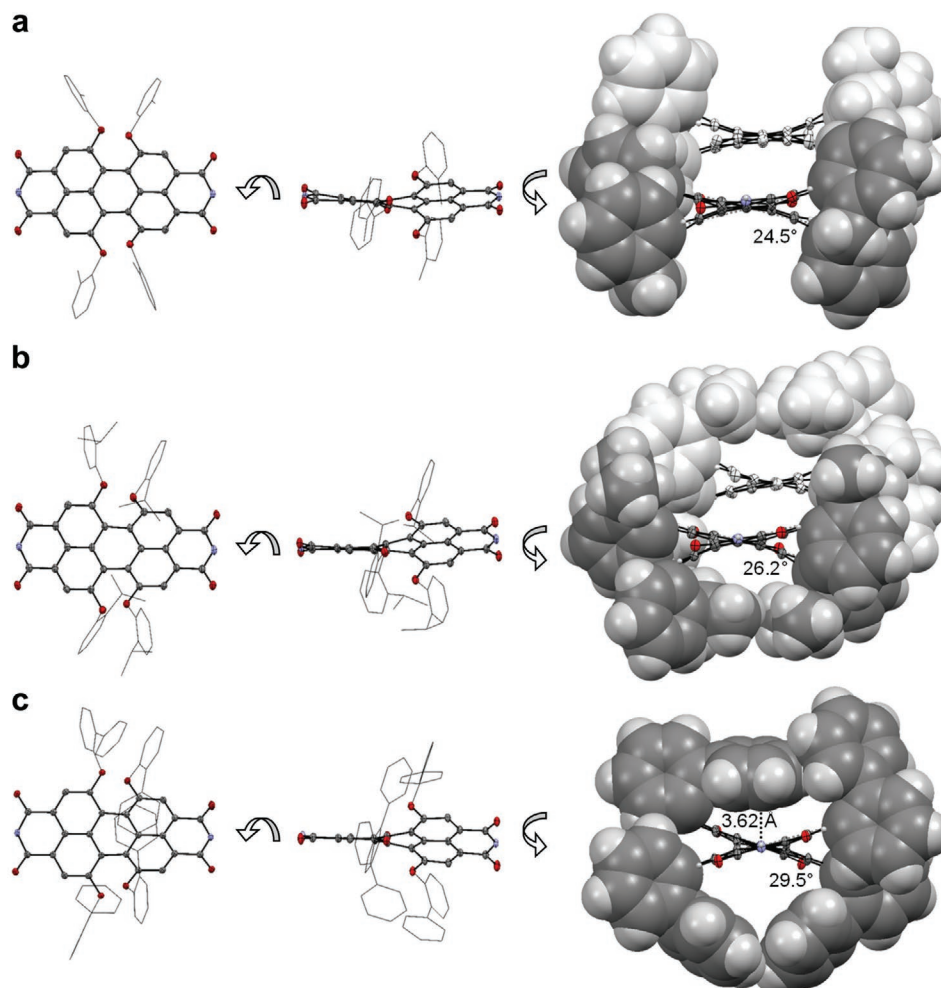


Figure 2. Molecular structures in top view (left), side view (middle), and along the PBIs N,N' -axis (right) of each P atropo-enantiomer taken from the solvent-free single crystal structures of a) **1(Me)**, b) **1(Pr)**, and c) **1(Ph)** illustrating the accessible and shielded sides of the PBI π -surfaces as well as the torsion angles of the two naphthalene subunits (gray). Phenoxys substituents are displayed in wireframe (left, middle) or space filling (right) while the ellipsoids of the PBI chromophore are set to 50% probability. Hydrogen atoms were partially omitted for clarity (C: gray, O: red, N: blue, H: white). The π -stacked nearest neighboring molecule is depicted in (a) and (b) in light gray.

the complementary π - π stacking motif of each PBI dye to both longitudinally displaced dyes in the next strand guided by the alternating M - and P -helical twist encoded in the PBIs within the double-strands. Interestingly, while the double-strands of **1(Me)** adopt a herringbone-like packing in the solid state, the chromophores of double- and single-strands of PBIs **1(Pr)** and **1(Ph)** are almost coplanar oriented in the crystal lattice (Figure 3).

The center-to-center distances of the parallel double-strands of PBIs **1(Me)** and **1(Pr)** are with 12.2 and 10.7 Å, respectively, even more separated than the single-strands of **1(Ph)** (9.89 Å), thereby affording negligible impact on the optical properties in the solid state (*vide infra*). In contrast to PBI J-aggregates observed in solution, the double-stranded arrangements do not show any helicity along the H-bonding axis. This originates from

Table 1. Structural parameters found in the solvent-free single crystal structures of **1(Me)**, **1(Pr)**, and **1(Ph)**.

| PBI | Space group | Core twist ^{a)} [°] | θ (C1–C12b–C12a–C12) ^{b)} [°] | θ (C13a–C12a–C12b–C13b) ^{b)} [°] | $r_{\pi-\pi}$ [Å] | $r_{\text{H-bond}}$ [Å] | $r_{\text{center-center}}^c)$ [Å] | $\theta_{\text{center-center}}^e)$ [°] |
|--------------|-------------|------------------------------|---|--|--------------------|-------------------------|-----------------------------------|--|
| 1(Me) | $P21/n$ | 24.5 | 26.59/27.52 | 21.66/21.98 | 3.48 | 2.87/2.89 | 7.88/8.24 | 29.6/27.9 |
| 1(Pr) | $P21/n$ | 26.2 ^{c)} | 27.20/30.16 ^{c)} | 22.80/25.18 ^{c)} | 3.51 ^{c)} | 2.83/2.94 ^{c)} | 7.37 | 29.8 |
| | | 26.3 ^{d)} | 27.87/28.54 ^{d)} | 23.37/24.72 ^{d)} | 3.51 ^{d)} | 2.83/2.94 ^{d)} | 8.59 | 25.4 |
| 1(Ph) | $P21/c$ | 29.5 | 29.10/32.85 | 25.45/26.90 | – | 2.86/2.92 | 9.89 | 65.9 |

^{a)}Angle between the PBI's two naphthalene subunits; ^{b)}Numbering of carbon atoms are according to Figure 1; ^{c)}Distances determined for the diastereomer with three phenoxys substituents facing in the same direction; ^{d)}Distances determined for the diastereomer with two residues facing upward and downward, respectively; ^{e)}For the definition of the center-to-center distance and the slip angle, see Figure 3.

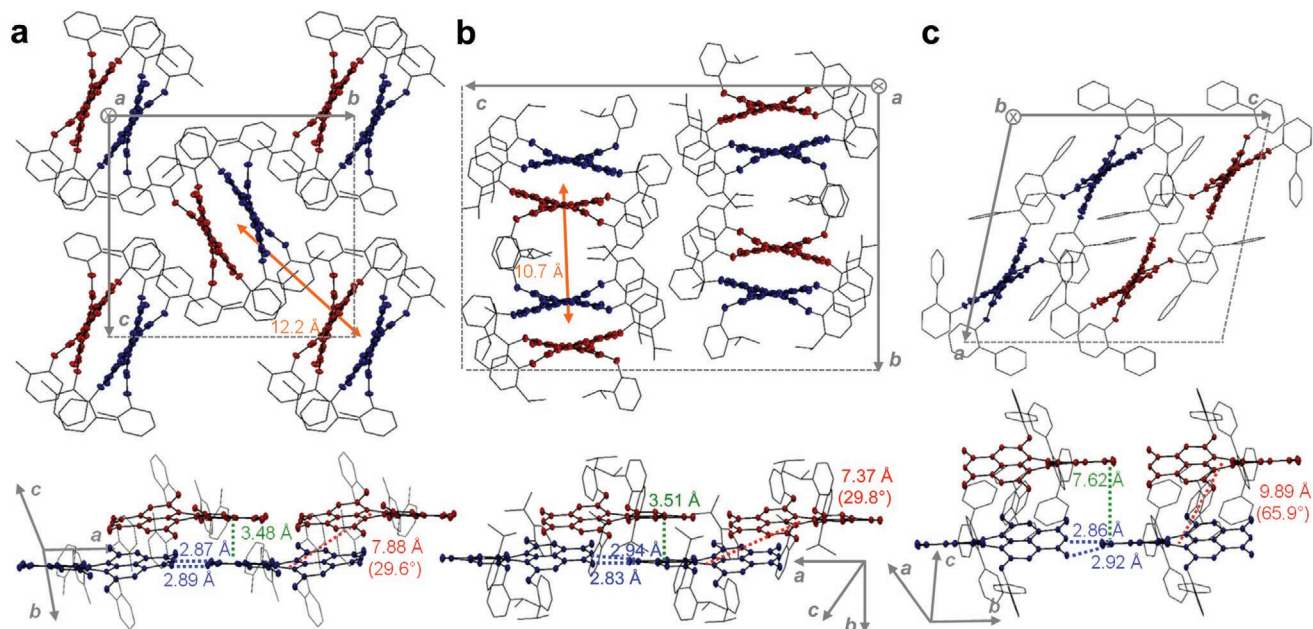


Figure 3. View onto the unit cell (top) of PBIs a) **1(Me)**, b) **1(Pr)**, and c) **1(Ph)** along the hydrogen-bonded PBI network of (a,b) double- and (c) single-stranded chromophores within their single crystal structures (ellipsoids set to 50% probability). Side view (bottom) onto the (a,b) double- and (c) single-stranded packing arrangements of hydrogen-bonded PBIs (a) **1(Me)**, (b) **1(Pr)**, and (c) **1(Ph)**. The PBI chromophores of *P* and *M* atropo-enantiomers are highlighted in blue and red, respectively, and the phenoxy substituents are presented in wireframe. Hydrogens are omitted for clarity. Lengths of hydrogen bonds (blue), distances of closest π - π interactions (green) as well as distances between individual strands (orange) and the centroids of the perylene cores (red) along with the corresponding slip angles are indicated as well.

the heterochiral assembly of *P* and *M* atropo-enantiomers that differs from the homochiral assembly found in solution.^[23,27]

This information from single crystal X-ray analysis is now most useful to elucidate the impact of the molecular packing of the PBIs dyes in single- and double-stranded arrangements on optical properties in the solid state (Figure S2, Supporting Information). The absorption and fluorescence properties of molecularly dissolved dyes in dichloromethane solution are similar to those reported for other tetraphenoxy PBI with longer solubilizing side chains.^[32] Thus, PBIs **1(Me)**, **1(Pr)**, and **1(Ph)** display almost identical absorption and fluorescence profiles with perfect mirror image band shapes (Figure S3, Supporting Information). Compared to tetraphenoxy PBIs without *ortho*-substituents we note a more defined vibronic progression that is attributed to the more restricted conformational space for the phenoxy groups.^[32] The absorption (λ_{abs}) and emission (λ_{em}) maxima are at 580–582 and 608–609 nm, respectively, giving rise to small Stokes shifts ($\Delta\tilde{\nu}_{\text{Stokes}}$) of only 760–820 cm^{-1} (Table 2). As expected, high fluorescence quantum yields (Φ_{F}) between 83% and 93% with corresponding fluorescence lifetimes (τ_{F}) between 6.62 ns for **1(Me)** and 7.41 ns for **1(Ph)** were determined (Table 2; Figure S4, Supporting Information). The high tinctorial strength of these PBIs is represented by high molar extinction coefficients (ϵ_{max}) of about $(42.3\text{--}45.0) \times 10^3 \text{ M}^{-1} \text{ cm}^{-1}$ as well as transition dipole moments (μ_{eg}) of 6.4–7.0 D of their S_0 – S_1 transition band (Figure S3, Supporting Information). A higher energy S_0 – S_2 transition can be observed at about 440 nm like for other twisted PBI chromophores.

In contrast to molecularly dissolved dyes, absorption and emission studies on solid-state samples are challenging for

chromophores with high tinctorial strength (ϵ_{max} , μ_{eg}). This holds in particular true for the thicker crystals (with thicknesses of several hundred nanometers) where their high optical densities (OD) leads to strong reabsorption which has a pronounced impact on both absorption and emission spectra as illustrated in Figure 4 for **1(Me)**.^[37] In Figure 4 we compare optical spectra obtained from spin-coated (10^{-4} M, CH_2CH_2 , 10 000 rpm) and solvent-treated vacuum-deposited (15 nm) thin films on quartz with spectra of an individual microcrystal grown from solution as well as an ensemble of single crystals obtained by gradient sublimation (for details see Supporting Information).

As could be expected from the single crystal structures of all PBIs, their microcrystals show strong anisotropy when studied with (fluorescence) polarization optical microscopy due to the unidirectional alignment of all chromophores in their respective crystal lattice (Figure 5; Figure S5, Supporting Information). However, while the gradient-sublimed crystalline material of PBIs **1(Me)** and **1(Pr)** show a dark bluish color, the powder of **1(Ph)** appears rather brownish/red (Figure S6, Supporting Information). This first indication for a smaller bathochromic shift of the absorption for single-stranded PBI **1(Ph)** is supported by the absorption profiles obtained from the reflectance spectra of gradient sublimed material in BaSO_4 trituration by the Kubelka–Munk theory^[38] (Table 2, Figure 6). We like to note, that due to grinding partial deaggregation occurs and therefore these spectra are contaminated by less perfectly ordered PBIs. While all PBIs show bathochromically shifted absorption maxima compared to the monomers in solution, this shift is with 320 cm^{-1} (11 nm) for **1(Ph)** less than half than for **1(Me)** with 1640 cm^{-1} (61 nm).

Table 2. Spectroscopic properties of **1(Me)**, **1(Pr)**, and **1(Ph)** as monomers in dichloromethane solution at 298 K as well as in the (crystalline) solid state.

| | PBI | λ_{abs} [nm] | λ_{em} [nm] | $\Phi_{\text{F}}^{\text{a}}$ [%] | $\tau_{\text{F}}^{\text{b}}$ [ns] | Rel. ^b [%] | χ^2 [1] |
|-------------|--------------|-----------------------------|----------------------------|----------------------------------|-----------------------------------|-----------------------|--------------|
| Solution | 1(Me) | 580 ^c | 608 ^c | 93 ^c | 6.62 ± 0.01 | 100 | 1.10 |
| | 1(Pr) | 582 | 609 | 83 | 6.78 ± 0.01 | 100 | 1.14 |
| | 1(Ph) | 580 | 609 | 91 | 7.41 ± 0.01 | 100 | 1.17 |
| Solid state | 1(Me) | 641 ^d | 685 ^e | 2.0 ^d | 0.25 ± 0.01 | 62 | 1.19 |
| | | | | (6) | 0.56 ± 0.04 | 33 | |
| | | | | | 1.92 ± 0.16 | 5 | |
| | 1(Pr) | 636 ^d | 674 ^e | 1.7 ^d | 0.26 ± 0.01 | 73 | 1.08 |
| | | | | (3) | 0.60 ± 0.05 | 25 | |
| | 1(Ph) | 591 ^d | 634 ^e | 15.4 ^d | 2.65 ± 0.01 | 100 | 1.32 |
| | | | (59) | | | | |

^a) Values in parenthesis are corrected for reabsorption according to ref. [41] using the respective microcrystal spectra; ^b) Fluorescence lifetimes (τ_{F}) and their relative contributions (Rel.) to the fluorescence decay curves after excitation with an EPL laser diode at 505.8 nm in front face setup with 22.5° geometry; ^c) Data taken von ref. [29]; ^d) Ensemble property of crystalline material obtained from gradient sublimation. Absorption spectra and maxima (λ_{abs}) where determined by applying the Kubelka–Munk theory^[38] on reflectance spectra of samples in BaSO₄ trituration; ^e) Microcrystal grown from solution on quartz substrate.

The same holds true for the microcrystal's emission spectra on quartz substrates (Figure 6). This can be rationalized by the missing additional exciton coupling (J_i) to the π -stacked nearest neighbor in double-strand PBIs in the H-bonded

chain arrangement of **1(Ph)** (Figure 3). A quantitative assessment by Kasha's exciton theory^[39] based on the point-dipole approximation applied on the data of the single crystal structures is provided in Figure S8 and Table S2 in the Supporting Information.

The absorption and excitation spectra of spin-coated and vacuum-deposited thin films of **1(Me)** exhibit the same onset and additionally allow us to study the spectral band shape.^[40] The thin-film spectra of **1(Me)** (Figure 4, blue line) are almost identical to those previously reported for **1(Me)** J-aggregate nanofibers in low-polar methylcyclohexane (MCH)^[29] with a narrowed absorption band and an about 70 nm red-shifted absorption maximum at 651 nm (Figure 4, gray dotted line). Fluorescence spectra of these thin films reveal a minor Stokes shift of only 160 cm⁻¹ ($\lambda_{\text{em}} = 658$ nm) for the thinnest spin-coated layer. With increasing sample thickness, the emission maximum is strongly falsified and red-shifted up to 749 nm for an ensemble of the crystalline material due to reabsorption (Figure 4), as OD increases in case of **1(Me)** by about 0.01 per nanometer PBI layer. Accordingly, the fluorescence maxima shift from the almost reabsorption-free spin-coated thin film (658 nm, OD = 0.04), the crystal grown from solution on quartz substrates (685 nm, OD = 0.16) up to the bulk material (749 nm, OD > 10) by almost 1850 cm⁻¹ (Figure 4). The emission maxima obtained from spectra of microcrystals grown from solution on quartz substrates of **1(Me)** (685 nm), **1(Pr)** (674 nm), and **1(Ph)** (634 nm) further support the observation, that double-stranded PBIs exhibit larger bathochromic shifts than their single-stranded counterpart (Table 2, Figure 6).

Even more challenging is the determination of the absolute quantum yield (Φ_{F}) of the crystalline pigments, as the measurement setup including an integrating sphere is fundamentally flawed due to multiple reflections within the sphere and the large amount of strongly absorbing pigment needed. Values for Φ_{F} of 2.0%, 1.7%, and 15.4% for PBIs **1(Me)**, **1(Pr)**, and **1(Ph)**, respectively, were determined upon excitation at 520 nm, which proves indisputably the higher solid-state

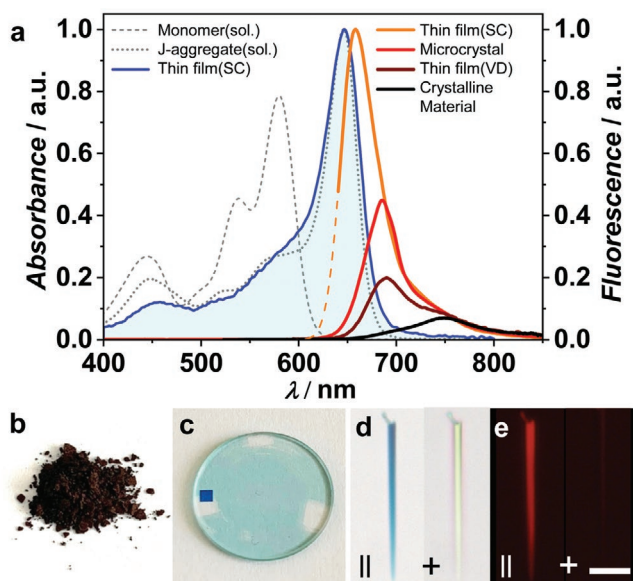


Figure 4. a) Absorption spectra of PBI **1(Me)** as monomer (gray dashed line; CH₂Cl₂), J-aggregate (gray dotted line, MCH) as well as spin-coated (SC) thin film on quartz (blue: 10 000 rpm). Emission spectra of spin-coated (orange) and solvent-treated vapor-deposited (VD, maroon) thin films as well as an individual microcrystal (red) and an ensemble of single crystals (black) obtained by gradient sublimation are presented. Correction of the blue wings of the fluorescence spectra of the spin-coated thin film are depicted as dashed orange line. Optical photographs of b) crystalline material as well as c) vacuum-deposited thin film under ambient light. d) Bright-field optical and e) fluorescence polarization microscope images of an individual microcrystal grown from solution on quartz substrates recorded with parallel-aligned polarizer (excitation) and analyzer (detection) oriented parallel (||) or perpendicularly (+) to the long crystal's axis. Scale bar: 10 μm.

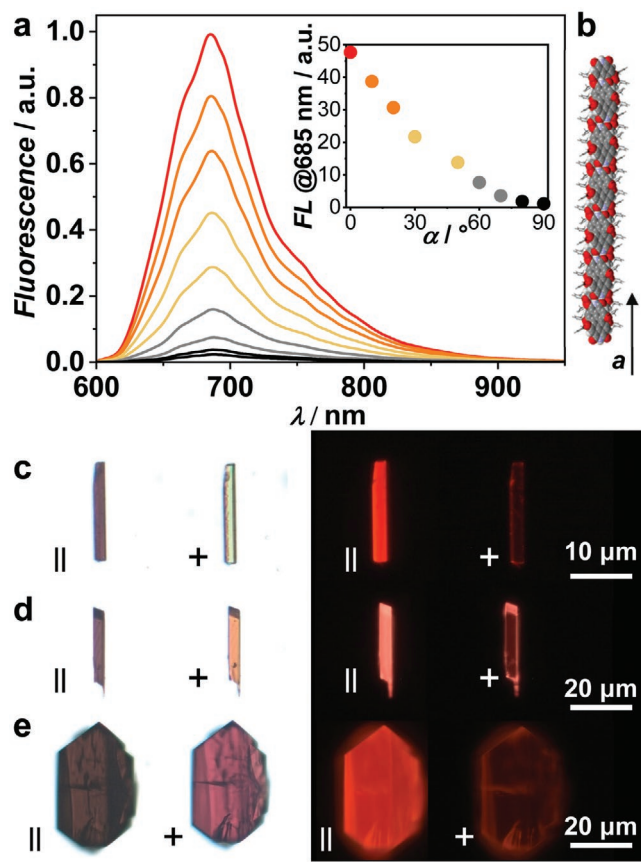


Figure 5. a) Polarization-dependent fluorescence spectra of a single crystal of PBI **1(Me)** obtained by gradient sublimation on quartz (c) with polarizer (excitation) and analyzer (detection) both oriented parallelly (red) or perpendicularly (black) with respect to the crystal's *a*-axis. Inset: respective change of the emission strength at 685 nm. b) Schematic molecular arrangement along the crystal's *a*-axis. Bright-field optical (left) and fluorescence (right) polarization microscope images of single crystals obtained by gradient sublimation of c) **1(Me)**, d) **1(Pr)**, and e) **1(Ph)** on quartz recorded with polarizer and analyzer oriented both parallelly (||) or perpendicularly (+) to the long crystal's axis.

fluorescence for the single-stranded, more heavily shielded PBI **1(Ph)** (Table 2; Figure S6, Supporting Information). Corrections for reabsorption^[41] were conducted yielding lower limits of 6%, 3% and 59% for **1(Me)**, **1(Pr)**, and **1(Ph)**, respectively, under the assumption that the emission profile of the individual microcrystals match the intrinsic solid-state fluorescence spectra (Figures 4 and 6). The value of 6% for **1(Me)**, albeit significantly reduced in comparison to the value of its J-aggregates in MCH solution (77%),^[29] might still be considered high because fast exciton diffusion in such J-type coupled chromophore architectures^[34,35] may lead to nonradiative relaxation on unavoidable trap sites in addition to other known relaxation pathways such as strong intermolecular electronic coupling^[42] or singlet fission into triplet states.^[22]

Further insights are obtained from fluorescence lifetime (τ_F) measurements for the crystalline materials, which can be recorded without any contamination by reabsorption. Fluorescence decay curves were recorded by time correlated single photon counting (TCSPC) with an EPL laser diode (505.8 nm)

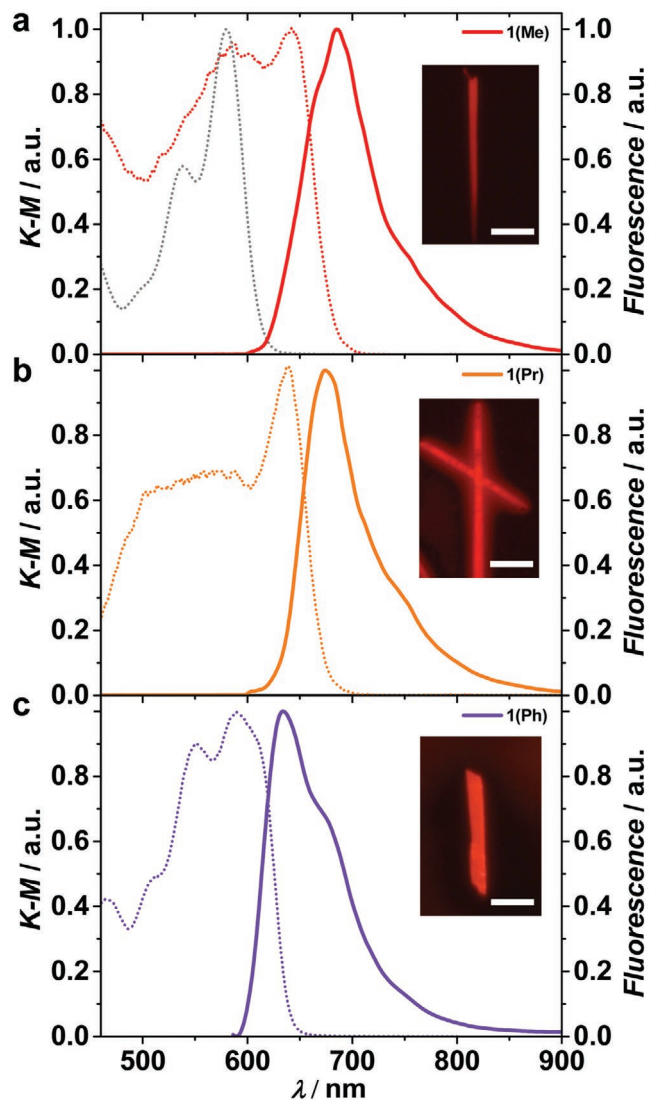


Figure 6. Normalized absorption spectra (dotted lines) determined by applying the Kubelka–Munk theory^[38] on the reflectance spectra of BaSO₄ trituration of PBIs a) **1(Me)** (red), b) **1(Pr)** (orange), and c) **1(Ph)** (violet). The monomer absorption spectrum of **1(Me)** in CH₂Cl₂ (gray dotted line) as well as the normalized fluorescence spectra (solid lines) of microcrystals grown from solution on quartz substrates are depicted as well. Inset: respective fluorescence polarization microscope images of the microcrystals grown on quartz substrates. Scale bar: 10 μ m.

in front-face geometry (22.5°) through detection at higher wavelengths than 711 nm (Figure S7, Supporting Information). While, for all PBIs the τ_F are significantly reduced, only single-stranded PBI **1(Ph)** shows still monoexponential decay with the longest τ_F = 2.65 ns (Table 2), which is about one third of the τ_F of monomers in solution (7.41 ns). By contrast, PBIs **1(Me)** and **1(Pr)** show multiexponential decay, whose major components are 0.25 and 0.26 ns, respectively. This tenfold decrease must be related to stronger electronic interactions within double-stranded packing arrangements of the less-shielded PBIs **1(Me)** and **1(Pr)** which beyond exciton coupling may also include charge transfer interactions.^[26]

3. Conclusion

In conclusion, we were able to grow solvent-free single crystals of three H-bonded tetraphenoxy-substituted perylene bisimide dyes by gradient sublimation in vacuum which adopt unique packing arrangements, i.e., double- (**1(Me)**, **1(Pr)**) and single- (**1(Ph)**) strands in the solid state of strongly J-coupled chromophores. These H-bonded chains are composed of only one atropo-enantiomer (*P* or *M*), with neighboring strands always containing the opposite stereoisomer. This heterochiral (“racemic”) π -stacking motif is in contrast to the narcissistic self-sorting^[43] observed for related dyes with solubilizing chains in solution and LC phases, where consistently homochiral helical aggregates composed of the same enantiomer are observed. Double-stranded systems show slip-stacked packing arrangement of π -stacked chromophores, while the individual strands of PBI **1(Ph)** are isolated by their phenyl-residues in *ortho*-position. Comparison of the spectroscopic properties in solution, crystalline powders as well as of individual single crystals revealed a decrease in effective fluorescence quantum yield in solid state compared to solution, however less severe for single-stranded PBI **1(Ph)** with 59% in comparison to double-stranded PBI **1(Me)** with 6%. Double-stranded J-aggregates of **1(Me)** and **1(Pr)** exhibit larger bathochromic shifts as well as strongly reduced fluorescence lifetimes (<0.26 ns) in contrast to single-stranded PBI **1(Ph)** (2.65 ns). These materials are interesting candidates for future studies on the exciton dynamics in well-defined 1D chains by ultrafast spectroscopy^[35] and for applications in light amplification^[44] and single crystal lasing.^[6]

4. Experimental Section

Synthesis and Characterization: The synthesis of precursors and of compound **1(Me)** has been described previously.^[29,46] The synthesis and characterization of **1(Pr)** and **1(Ph)** is given in the Supporting Information.

Spectroscopy in Solution: UV/vis absorption spectra were measured on a Lambda 950 spectrophotometer (Perkin-Elmer). Fluorescence spectra were recorded on an Edinburgh Instruments FLS980-D2D2-ST spectrometer and were corrected against the photomultiplier sensitivity and the lamp intensity. Fluorescence lifetimes were determined with an EPL picosecond pulsed diode laser ($\lambda_{\text{ex}} = 505.8$ nm) for TCSPC with an Edinburgh Instruments FLS980-D2D2-ST spectrometer. Measurements were performed using 1 mm or 1 cm quartz cuvettes (SUPRASIL) and spectroscopic solvents (Merck). UV/vis absorption and emission spectra of **1(Me)**, **1(Pr)**, and **1(Ph)** were measured in CH_2Cl_2 and MCH at RT.

Spectroscopy in Solid State: Optical investigations were performed on a Zeiss Axio Imager optical polarization microscope. Emission spectra of individual single crystals were measured on the same instrument with an integrated Zeiss CCD spectrometer customized by A.S. & Co with a spot resolution of up to $4 \times 4 \mu\text{m}^2$. Thin films for optical investigations of **1(Me)** were prepared as follows: 1) A saturated solution of **1(Me)** in CHCl_3 was filtered (polytetrafluoroethylene (PTFE) filters, 0.22 μm). Then spin-coating was performed at 10 000 rpm, 5000 rpm s^{-1} for 60 s. Suprasil quartz plates (Type: 202-QS) were used as substrates. 2) A layer of 15 nm of **1(Me)** were deposited with a rate of 0.2 $\text{\AA} \text{s}^{-1}$ at a pressure of $<2 \times 10^{-6}$ mbar on heated (130 °C) Suprasil quartz plates (Type: 202-QS) with an OPTIvap-XL deposition tool (CreaPhyS GmbH) while the substrate stage rotated for increased homogeneity. These freshly processed film was shortly rinsed on a spin-coater (3000 rpm, 60 s) with a solution of *ortho*-dichlorobenzene/diiodooctane (99:1) under inert atmosphere (M.Braun Inertgas Systeme GmbH, UNIlab Pro, $c(\text{O}_2) < 1$ ppm, $c(\text{H}_2\text{O}) < 1$ ppm) to complete full transformation.

Microcrystal Growth: Microcrystals of **1(Me)** and **1(Pr)** were grown based on the slow evaporation method.^[46] A saturated solution of PBI was prepared and filtered (PTFE, 0.22 μm) and then mixed with MeOH in a ratio of 1:1 (v/v). Screw caps were filled with 250 μL of CHCl_3 :MeOH in a ratio of 1:1 (v/v). Suprasil quartz plates (Type: 202-QS) were used as substrates. It took three days for the solvent to evaporate completely from the closed vessels. Single crystals of **1(Ph)** were grown by drop-casting the compound on quartz plates from a CHCl_3 solution (2 mg mL^{-1}) and subsequent solvent vapor annealing with CHCl_3 for 30 min.

Single Crystal Growth: Solvent-free single crystals of **1(Me)**, **1(Pr)**, and **1(Ph)** were obtained by vacuum sublimation, using a thermal gradient sublimation system of HTM Reetz GmbH. About 5 mg of raw material were placed into a standard NMR tube as a fine powder. Small pieces of the (100) wafers with a width of 2–3 mm and a length off around 10 mm were placed into the NMR tube (polished side facing up). The NMR tube in turn was positioned centrally between the 1st and the 2nd heating zone of the thermal gradient sublimation system. Prior to heating, the system was evacuated for about 2 h until a pressure of at least 2×10^{-6} mbar was reached. Then the 1st and the 2nd heating zone were heated up with a rate of ≈ 10 K min^{-1} . The experiment was stopped when single crystals of sufficient size had grown, mainly on the edges of the wafer pieces facing toward the organic material.

X-Ray Diffraction: X-ray diffraction measurements of **1(Me)**, **1(Pr)**, and **1(Ph)** were performed on a D8 Quest Kappa diffractometer of Bruker working with a Photon100 complementary metal-oxide-semiconductor (CMOS) or with a Photon II CMOS detector, Cu $K\alpha$ radiation (0.15418 nm) and at a temperature of 100 K. Crystal structures were solved using direct methods, expanded by Fourier techniques and were refined with the Shelx software package.^[47] Anisotropic refinement was performed on nonhydrogen atoms, while hydrogen atoms were included in the structure factor calculation on geometrically idealized positions. Powder XRD measurements were performed on a D8 Discover (Bruker) with a LynxEye-1D-Detector using Cu $K\alpha$ radiation (0.15418 nm). Powder XRD patterns were measured of the crystalline bulk material of **1(Me)**, **1(Pr)**, and **1(Ph)** obtained by thermal gradient sublimation. To ensure high crystallinity of the investigated solid-state materials powder XRD measurements were performed on the purified and solvent-free PBIs after thermal gradient sublimation and compared them to the simulated diffraction patterns of their respective single crystal structures. The complementarity of these patterns without any significant additional peaks led to the conclusion that the majority of bulk material inherits the desired molecular packing as in the single crystal structures.

Supporting Information

Supporting Information is available from the Wiley Online Library or from the author.

Acknowledgements

The authors thank the Deutsche Forschungsgemeinschaft (DFG) for financial support by the research grant WU 317/18-1.

Conflict of Interest

The authors declare no conflict of interest.

Keywords

fluorescence, J-aggregates, perylene bisimides, reabsorption, single crystal structure

Received: June 8, 2020
Published online: June 25, 2020

- [1] P. Erk, H. Hengelsberg, M. F. Haddow, R. van Gelder, *CrystEngComm* **2004**, *6*, 474.
- [2] R. Ramakrishnan, M. A. Niyas, M. P. Lijina, M. Hariharan, *Acc. Chem. Res.* **2019**, *52*, 3075.
- [3] G. R. Desiraju, *Angew. Chem., Int. Ed.* **2007**, *46*, 8342; *Angew. Chem.* **2007**, *119*, 8492.
- [4] S. Saha, M. K. Mishra, C. M. Reddy, G. R. Desiraju, *Acc. Chem. Res.* **2018**, *51*, 2957.
- [5] P. Yu, Y. Zhen, H. Dong, W. Hu, *Chem* **2019**, *5*, 2814.
- [6] J. Gierschner, S. Varghese, S. Y. Park, *Adv. Opt. Mater.* **2016**, *4*, 348.
- [7] K. Hunger, M. U. Schmidt, *Industrial Organic Pigments*, 4th ed., Wiley-VCH, Weinheim, Germany **2018**.
- [8] G. Klebe, F. Graser, E. Hädicke, J. Berndt, *Acta Crystallogr., Sect. B: Struct. Sci.* **1989**, *45*, 69.
- [9] P. M. Kazmaier, R. Hoffmann, *J. Am. Chem. Soc.* **1994**, *116*, 9684.
- [10] F. Würthner, *Chem. Commun.* **2004**, 1564.
- [11] C. Yan, S. Barlow, Z. Wang, H. Yan, A. K.-Y. Jen, S. R. Marder, X. Zhan, *Nat. Rev. Mater.* **2018**, *3*, 18003.
- [12] A. Nowak-Król, K. Shoyama, M. Stolte, F. Würthner, *Chem. Commun.* **2018**, *54*, 13763.
- [13] S.-K. Jung, J. H. Heo, B. M. Oh, J. B. Lee, S.-H. Park, W. Yoon, Y. Song, H. Yun, J. H. Kim, S. H. Im, O.-P. Kwon, *Adv. Funct. Mater.* **2020**, *30*, 1905951.
- [14] A. Nowak-Król, F. Würthner, *Org. Chem. Front.* **2019**, *6*, 1272.
- [15] X. Cao, S. Bai, Y. Wu, Q. Liao, Q. Shi, H. Fu, J. Yao, *Chem. Commun.* **2012**, *48*, 6402.
- [16] M. G. Ramírez, S. Pla, P. G. Boj, J. M. Villalvilla, J. A. Quintana, M. A. Díaz-García, F. Fernández-Lázaro, Á. Sastre-Santos, *Adv. Opt. Mater.* **2013**, *1*, 933.
- [17] P. Lova, V. Grande, G. Manfredi, M. Patrini, S. Herbst, F. Würthner, D. Comoretto, *Adv. Opt. Mater.* **2017**, *5*, 1700523.
- [18] M. R. Wasielewski, *Acc. Chem. Res.* **2009**, *42*, 1910.
- [19] F. Würthner, C. R. Saha-Möller, B. Fimmel, S. Ogi, P. Leowanawat, D. Schmidt, *Chem. Rev.* **2016**, *116*, 962.
- [20] T. Brixner, R. Hildner, J. Köhler, C. Lambert, F. Würthner, *Adv. Energy Mater.* **2017**, *7*, 1700236.
- [21] M. Gsänger, J. H. Oh, M. Könemann, H. W. Höffken, A.-M. Krause, Z. Bao, F. Würthner, *Angew. Chem.* **2010**, *122*, 752; *Angew. Chem., Int. Ed.* **2010**, *49*, 740.
- [22] S. W. Eaton, L. E. Shoer, S. D. Karlen, S. M. Dyar, E. A. Margulies, B. S. Veldkamp, C. Ramanan, D. A. Hartzler, S. Savikhin, T. J. Marks, M. R. Wasielewski, *J. Am. Chem. Soc.* **2013**, *135*, 14701.
- [23] Z. Xie, B. Xiao, Z. He, W. Zhang, X. Wu, H. Wu, F. Würthner, C. Wang, F. Xie, L. Liu, Y. Ma, W.-Y. Wong, Y. Cao, *Mater. Horiz.* **2015**, *2*, 514.
- [24] J. Zhou, W. Zhang, X.-F. Jiang, C. Wang, X. Zhou, B. Xu, L. Liu, Z. Xie, Y. Ma, *J. Phys. Chem. Lett.* **2018**, *9*, 596.
- [25] E. Sebastian, A. M. Philip, A. Benny, M. Hariharan, *Angew. Chem.* **2018**, *130*, 15922; *Angew. Chem., Int. Ed.* **2018**, *57*, 15696.
- [26] N. J. Hestand, F. C. Spano, *Chem. Rev.* **2018**, *118*, 7069.
- [27] T. E. Kaiser, H. Wang, V. Stepanenko, F. Würthner, *Angew. Chem.* **2007**, *119*, 5637; *Angew. Chem., Int. Ed.* **2007**, *46*, 5541.
- [28] T. E. Kaiser, V. Stepanenko, F. Würthner, *J. Am. Chem. Soc.* **2009**, *131*, 6719.
- [29] Z. Xie, V. Stepanenko, B. Fimmel, F. Würthner, *Mater. Horiz.* **2014**, *1*, 355.
- [30] V. Grande, B. Soberats, S. Herbst, V. Stepanenko, F. Würthner, *Chem. Sci.* **2018**, *9*, 6904.
- [31] S. Herbst, B. Soberats, P. Leowanawat, M. Lehmann, F. Würthner, *Angew. Chem.* **2017**, *129*, 2194; *Angew. Chem., Int. Ed.* **2017**, *56*, 2162.
- [32] S. Herbst, B. Soberats, P. Leowanawat, M. Stolte, M. Lehmann, F. Würthner, *Nat. Commun.* **2018**, *9*, 2141.
- [33] M. Hecht, T. Schlossarek, M. Stolte, M. Lehmann, F. Würthner, *Angew. Chem.* **2019**, *131*, 13113; *Angew. Chem., Int. Ed.* **2019**, *58*, 12979.
- [34] A. Merdasa, Á. J. Jiménez, R. Camacho, M. Meyer, F. Würthner, I. G. Scheblykin, *Nano Lett.* **2014**, *14*, 6774.
- [35] J. Dostál, F. Fennel, F. Koch, S. Herbst, F. Würthner, T. Brixner, *Nat. Commun.* **2018**, *9*, 2466.
- [36] F. Würthner, *Pure Appl. Chem.* **2006**, *78*, 2341.
- [37] Remark: This is even more severe for J-type aggregates which show strong exchange narrowing as well as even smaller Stokes shift, making it almost impossible to obtain precise data without any falsification by reabsorption.
- [38] P. Kubelka, F. Munk, *Z. Tech. Phys.* **1931**, *12*, 593.
- [39] M. Kasha, *Radiat. Res.* **1963**, *20*, 55.
- [40] Remark: This comparison was unfortunately not possible for **1(Pr)** and **1(Ph)**, as the optical properties of their thin films did not matched those of (micro-)crystals.
- [41] T.-S. Ahn, R. O. Al-Kaysi, A. M. Müller, K. M. Wentz, C. J. Bardeen, *Rev. Sci. Instrum.* **2007**, *78*, 086105.
- [42] S. Varghese, S. K. Park, S. Casado, R. Resel, R. Wannemacher, L. Lüler, S. Y. Park, J. Gierschner, *Adv. Funct. Mater.* **2016**, *26*, 2349.
- [43] M. M. Safont-Sempere, G. Fernández, F. Würthner, *Chem. Rev.* **2011**, *111*, 5784.
- [44] S. Betzold, S. Herbst, A. A. P. Trichet, J. M. Smith, F. Würthner, S. Höfling, C. P. Dietrich, *ACS Photonics* **2018**, *5*, 90.
- [45] C.-C. You, F. Würthner, *J. Am. Chem. Soc.* **2003**, *125*, 9716.
- [46] A. Liess, M. Stolte, T. He, F. Würthner, *Mater. Horiz.* **2016**, *3*, 72.
- [47] G. M. Sheldrick, *Acta Crystallogr., Sect. A: Found. Crystallogr.* **2008**, *64*, 112.